

Theoretical characterization of a model of aragonite crystal orientation in red abalone nacre

S.N. Coppersmith, P.U.P.A. Gilbert, and R.A. Metzler

Department of Physics, University of Wisconsin, Madison, WI 53706

Abstract. Nacre, commonly known as mother-of-pearl, is a remarkable biomineral that in red abalone consists of layers of 400-nm thick aragonite crystalline tablets confined by organic matrix sheets, with the (001) crystal axes of the aragonite tablets oriented to within $\pm 12^\circ$ from the normal to the layer planes. Recent experiments demonstrate that this orientational order develops over a distance of tens of layers from the prismatic boundary at which nacre formation begins.

Our previous simulations of a model in which the order develops because of differential tablet growth rates (oriented tablets growing faster than misoriented ones) yield patterns of tablets that agree qualitatively and quantitatively with the experimental measurements. This paper presents an analytical treatment of this model, focusing on how the dynamical development and eventual degree of order depend on model parameters. Dynamical equations for the probability distributions governing tablet orientations are introduced whose form can be determined from symmetry considerations and for which substantial analytic progress can be made. Numerical simulations are performed to relate the parameters used in the analytic theory to those in the microscopic growth model. The analytic theory demonstrates that the dynamical mechanism is able to achieve a much higher degree of order than naive estimates would indicate.

1. Introduction

Nacre, or mother-of-pearl, is a biomineral that attracts the attention of materials scientists, biologists, and mineralogists as well as physicists because of its remarkable mechanical properties and its incompletely elucidated formation mechanisms [1–5]. Aragonite, a hard but brittle orthorhombic $CaCO_3$ polymorph, accounts for 95% of nacre’s mass, yet nacre is 3000 times tougher than aragonite [6]. No synthetic composites outperform their components by such large factors. It is therefore of great interest to understand the mechanisms governing nacre formation.

Nacre is a layered composite in which organic matrix (OM) sheets alternate with aragonite layers, each of which consists of tablets of irregular polygonal shape that completely fill the space between preformed OM layers. In red abalone, the OM layers are 30-nm thick, and the aragonite tablets are of thickness 400-500nm and width 5-6 microns [7,8]. The aragonite tablets are crystalline and oriented with their (001) crystal axes within $\pm 12^\circ$ from the normal to the layer plane [8,9]. TEM and AFM measurements

have shown that the OM has pores through which aragonite can grow [10, 11], and x-ray and x-ray photoelectron emission spectromicroscopy (X-PEEM) measurements demonstrate that nacre has stacks of co-oriented tablets [7, 8, 12], consistent with the hypothesis that aragonite crystals grow through pores in the OM sheets.

Growth through pores explains how crystal orientation of the aragonite tablets is maintained between layers in the material, but it does not necessarily explain the physical mechanism giving rise to the orientational alignment in the first place. It is common belief in the biomineralization field that the alignment of the aragonite crystal c -axes is due to microscopic chemical templation by the OM [1, 13], with organic molecules providing surfaces that promote aragonite nucleation with preferred orientations. However, it is not obvious why such a mechanism would lead to a high degree of orientational order of the c -axes but not of the a or b axes of the aragonite tablets. Moreover, Ref. [8] reports x-ray photoelectron emission spectromicroscopy (X-PEEM) and microbeam X-ray diffraction that probe the degree of orientational alignment of the aragonite c -axes [7, 14] and demonstrate that the orientational alignment of the aragonite tablets increases systematically over a length scale of tens of microns starting from the prismatic boundary at which nacre growth originates. As discussed in Ref. [8], this observation suggests that the aragonite crystal orientation is the result of a dynamical process.

In Refs. [8, 15] a dynamical model is proposed for the development of orientational order of the aragonite tablets in nacre in which the presence of co-oriented stacks of tablets plays an essential role, and the ordering arises because oriented tablets grow faster than misoriented ones. Refs. [8, 15] present numerical simulations of the model that successfully reproduce several different aspects of the pattern of tablet orientations in red abalone nacre measured using X-PEEM. This paper presents a more detailed investigation of the model and its behavior, including closed-form analytic results that apply in the limit that the probability of nucleating a tablet with orientation different from the one immediately below is small, which, based on comparison to the X-PEEM results, is the physically relevant regime. We find that the dynamical ordering mechanism can lead to a remarkably high degree of orientation of the tablet c -axes, because the width of the distribution of tablet orientations decreases very strongly as the fraction of tablets that nucleate with the “wrong” orientation decreases.

The analytic characterization of the model uses methods similar to those used to study mutation-selection models in population biology [16–18]. However, the analytic formulation involves some parameters whose relationship to those of the growth model is not determined in Ref. [8]. These parameters are examined here, and it is shown that this relationship is not trivial. The relationship between the parameter sets depends on the spatial arrangement of the nucleation sites, and some aspects are quite insensitive to changes in the values of the microscopic parameters. Numerical simulations and mean-field arguments are used to relate the parameters in the analytic probabilistic model to the parameters in the original growth model for the case when the nucleation sites are chosen randomly with uniform probability on each layer.

The paper is organized as follows. Section 2 presents the model, while section 3 presents the analysis of the probabilistic model that enables one to understand qualitatively some features of the behavior, using methods that have been developed to study models relevant to population biology [16–22]. The fixed point behavior is discussed in subsection 3.1, while the dynamical evolution is discussed in subsection 3.2. Section 4 discusses the relationships between the parameters of the growth model to those of the model for the probability distribution for tablet orientations. Sec. 5 is a discussion, and the conclusions are presented in Sec. 6. Appendix A presents additional details of the arguments justifying the functional forms of the equations used in the main text.

2. The model

Figure 1 illustrates the basic mechanism of nacre growth [1, 10, 23]. First, organic matrix sheets spaced by approximately 0.4 microns are created. Crystalline aragonite tablets then nucleate on the first layer at uncorrelated random locations and grow while confined by the organic matrix sheets. The crystals in this layer continue to grow and fill out the space in the layer [1, 24, 25]. Each nacre tablet in a given layer nucleates and then grows until it reaches confluence with a neighboring tablets, so that the resulting tablet pattern resembles a Voronoi construction [2, 5], with tablet in-plane width of order 5 microns. The crystal orientation of each tablet is highly probable to be the same as that of the tablet directly below its nucleation site [10, 11, 26], which reflects the presence of pores in the organic matrix (typically with diameter $\sim 5 - 50$ nm) through which aragonite crystals can grow. As discussed in [2, 8], there is one nucleation site per tablet, with an identifiable structure in the organic matrix that is large enough to have one or more pores going through it.

The model that we examine here assumes that growth in a given layer is completed before tablets in the succeeding layer are nucleated, and that the positions of nucleation sites in all successive layers are nucleated at locations that are uncorrelated with those in the preceding layers. The growth rates in the first layer are chosen uniformly at random in the interval $[1 - \delta/2, 1 + \delta/2]$, and the tablets in each layer grow to confluence. With probability $1 - \epsilon$ a tablet has the same growth rate as the tablet below its nucleation site, while with probability ϵ the tablet is assigned a growth rate chosen uniformly at random from the range $[1 - \delta/2, 1 + \delta/2]$. Appendix A presents the arguments that these choices of the probability distributions are natural, given the geometry of the experimental system. The version of the model used here and in Ref. [15] is simpler than that examined in Ref. [8], which explicitly models columnar nacre by assuming that growth in a given layer is not completed before tablets in the succeeding layer are nucleated, so that nucleation sites in successive layers must be within a certain in-plane distance and are thus correlated; it is theoretically more attractive because it requires the specification of one fewer parameter. Ref. [15] presents numerical simulations of the model and experimental data on the pattern of tablet orientations in red abalone

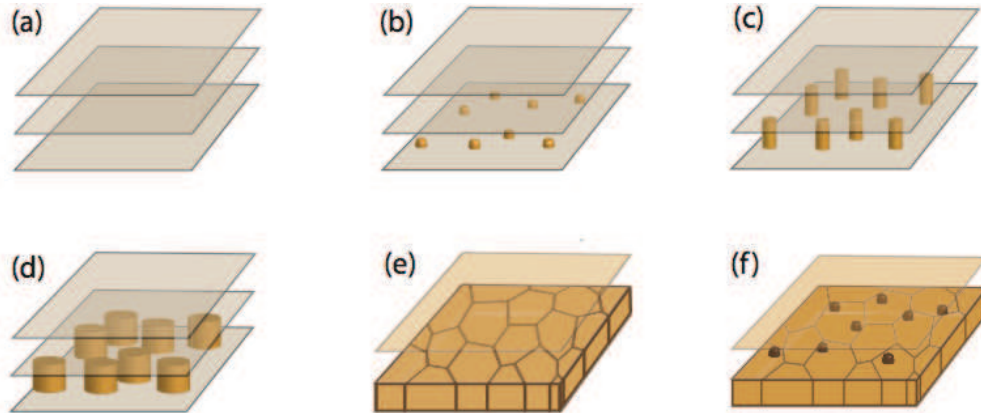


Figure 1. Schematic of growth of sheet nacre, which exhibits layer-by-layer growth. (a) Scaffolding of organic matrix sheets is created. (b) Crystalline aragonite tablets are nucleated at random positions in the first layer of pre-existing scaffolding of organic matrix sheets. (c-e) Aragonite tablets are confined by organic matrix sheet in the next layer, but grow within the layer until they reach confluence. (f) Aragonite tablets are nucleated at random positions in the next layer. With high probability, the nucleated tablet has the same crystal orientation as that of the tablet directly below the nucleation site [10, 11, 26].

nacre, and demonstrates that numerical simulations of this model using parameter values $\epsilon = 0.015$ and $\delta = 0.25$ yields good agreement with the experimental measurements on nacre from red abalone, *Haliotis rufescens*.

The next section presents an analytic treatment of the behavior of the probability distribution function governing the density of tablets of different orientations as a function of the distance from the prismatic boundary.

2.1. Growth model used for simulations

This paper reports simulation of a model in which nucleation sites are placed randomly on a square calculational domain with open boundary conditions. In each layer, the rate of growth of each tablet is chosen at random from a uniform distribution in the range $[1 - \delta/2, 1 + \delta/2]$. The tablets nucleate simultaneously and grow to confluence before successive layers are nucleated. The resulting pattern of tablet boundaries in each layer is a multiplicatively weighted Voronoi construction [27–29]. Variations in the in-plane extent of each tablet within each individual layer are ignored, so that the volume of a given tablet is the product of its area and the layer separation. Because faster-growing tablets tend to take up a greater fraction of the area, and because a tablet will nucleate with the same velocity as the tablet below it with probability $1 - \epsilon$, when ϵ is small, there is a tendency for faster-growing tablets to take up more and more of the total area (and hence volume) as the growth proceeds. The ordering is not perfect, however, because some misoriented tablets are nucleated.

3. Effective theory for the evolution of probability distribution of tablet orientations

The theory in this section is formulated in terms of crystal orientations, as opposed to the formulation in terms of growth rates in the previous section. It is useful to consider this formulation because the X-PEEM experiments measure crystal orientations as opposed to growth rates, so comparison of theoretical predictions to experimental results is facilitated. Motivated by the ordering of tablet c-axis orientations observed experimentally, our model posits that variability in the orientations of the c-axes of the tablets gives rise to variability in the tablet growth rates, with tablets with c-axes aligned perpendicular to the layer plane growing the fastest.

This section presents and analyzes dynamical equations that govern the evolution of the probability distribution describing the number of tablets with different crystal orientations. These equations can be solved analytically in the limit that the fraction of misoriented tablets is very small, which is the parameter regime relevant to the experiments of Ref. [8]. We find that the geometry of the dynamical model leads to the result that the distribution of tablet orientations (or, equivalently, growth rates) has an extremely sharp peak whose width is exponentially small in ϵ , the fraction of misoriented tablets.

The analytic theory presented here for the evolution of tablet orientations in nacre is closely related to mutation-selection models studied in the context of population biology [17–22]. The faster growth of tablets of a particular orientation is analogous to the process of selection in population biology, where species with higher fitness reproduce faster than species with lower fitness. In the growth model examined in this paper, after all the tablets in a given layer grow to confluence, the next layer nucleates. When a tablet in the next layer nucleates, one of two things can happen. The first, more likely, possibility is that the nucleated tablet has the same orientation as the tablet directly below its nucleation site (analogous to inheritance, where the descendant has the same fitness as the parent), while the second is that the tablet has a randomly chosen orientation (analogous to mutation, where the fitness of the descendant differs from that of the ancestor by a random amount). Selection in the growth model is reflected in the tendency for a larger fraction of the area to be filled with tablets with higher growth rates, which increases the probability that a given randomly located nucleation point is located over a tablet with a higher growth rate.

The analytic theory presented here is similar to Ginzburg-Landau theories [30] often used in statistical physics [31] to describe phase transitions in condensed matter systems, in that the functional forms follow from symmetry and dimensionality considerations and may involve unknown coefficients. Even if the numerical values of these coefficients are not known, the analytic theory is very useful for obtaining insight into the interplay between the various parameters in the problem. However, additional insight is obtained if the Ginzburg-Landau parameters can be related to the parameters of the growth model described above in Sec. 2.1, which is done in Sec. 4 using a simple mean-field

theory and also by comparing the predictions of the analytical model to the results of numerical simulations.

We define $\phi_\ell(\gamma)d\gamma$ to be the fraction of tablets in layer ℓ that are misoriented from the layer normal by angles that are between γ and $\gamma + d\gamma$. We assume that tablets with $\gamma = 0$ have the largest rate of growth, so their share of the area in layer $\ell + 1$ will tend to be greater than in layer ℓ , thus leading to a larger fraction of tablets with crystal axes oriented parallel to the layer normal; the function $w(\gamma)$ governs this tendency. We define $\chi_\ell(\gamma)d\gamma$ to be the fraction of the area in layer ℓ after its growth is completed that is oriented in the range of angles between γ and $\gamma + d\gamma$ from the layer normal, and that

$$\chi_\ell(\gamma) = \frac{1}{N_\ell} w(\gamma) \phi_\ell(\gamma) , \quad (1)$$

where, for each ℓ , the normalization factor N_ℓ is determined by the normalization of the probability:

$$1 = \int_0^\pi d\gamma \chi_\ell(\gamma) \quad (2)$$

$$\Rightarrow N_\ell = \int_0^\pi d\gamma w(\gamma) \phi_\ell(\gamma) . \quad (3)$$

The maximum growth rate is at $\gamma = 0$, and one expects $w(\gamma)$ to have a quadratic maximum at $\gamma = 0$. We will scale $w(\gamma)$ so that $w(0) = 1$. We assume that $w(\gamma)$ is a function only of γ (in other words, that it depends only on the degree of misorientation of the c-axis and not on the orientation of the a and b axes). One expects the dependence of $w(\gamma)$ on γ near its maximum at $\gamma = 0$ to be quadratic, which, if the distribution is not too broad, can be approximated as a Gaussian,

$$w(\gamma) \propto \left(1 - \frac{\alpha\gamma^2}{2}\right) \approx e^{-\alpha\gamma^2/2} , \quad (4)$$

where α is a numerical coefficient. The tendency for fast-growing tablets to take up an increasing fraction of the total tablet area is analogous to the effects of selection in population biology, where organisms with higher fitness tend to comprise an increasing fraction of the population.

We then assume that most of the tablets that nucleate in layers above the first layer have the same crystal orientations as those of the tablets just below their nucleation sites, but that there is a small probability ϵ that a tablet nucleates with a value of γ that is chosen at random from a normalized probability distribution $f(\gamma)$. The nucleation of misoriented tablets in the nacre growth model is analogous to the effects of mutation in a population genetics model.

The combination of these growth and nucleation terms leads to a dynamical equation governing the behavior of $\phi_\ell(\gamma)$:

$$\begin{aligned} \phi_\ell(\gamma) &= \epsilon f(\gamma) + (1 - \epsilon) \chi_\ell(\gamma) \\ &= \epsilon f(\gamma) + \frac{1}{N_\ell} (1 - \epsilon) \phi_{\ell-1}(\gamma) w(\gamma) . \end{aligned} \quad (5)$$

To complete the definition of the model, one must specify an appropriate form for $f(\gamma)$, the function describing the distribution of angles of misoriented tablet orientations.

We will show below that the behavior depends only on the properties of $f(\gamma)$ as $\gamma \rightarrow 0$. In Appendix A it is found that the generic behavior for $f(\gamma)$ for small γ is for $f(\gamma)$ to be proportional to γ as $\gamma \rightarrow 0$. This result is intuitively reasonable for this system geometry because the angular area between γ and $\gamma + d\gamma$ is proportional to γ as $\gamma \rightarrow 0$. At some points in the analytic treatment below, we will choose the specific, mathematically convenient form $f(\gamma) = \beta\gamma e^{-\beta\gamma^2/2}$. This choice does not affect any of the results, because the behavior of $f(\gamma)$ as $\gamma \rightarrow 0$ determines the asymptotic behavior.

We characterize the behavior of this model using the methods of Refs. [16–18]. First we note that when $\epsilon = 0$, so that the co-orientation of tablets in successive layers is perfect, this model is easily solved for any initial distribution, $\phi_1(\gamma)$. Since increasing ℓ by one multiplies the un-normalized $\phi_\ell(\gamma)$ by $w(\gamma)$, it follows immediately that

$$\phi_\ell(\gamma) \propto \phi_1(\gamma)(w(\gamma))^{\ell-1} . \quad (6)$$

(Note that it is sufficient to compute the un-normalized distribution since the normalization factor for any given ℓ can always be obtained via Eq. (2).) The long-time behavior for any $w(\gamma)$ with a single quadratic maximum at $\gamma = 0$ depends only on the curvature in $w(\gamma)$ near $\gamma = 0$. For the specific choice $w(\gamma) = \exp(-\alpha\gamma^2/2)$, one finds $\phi_\ell(\gamma) \propto \phi_1(\gamma) \exp(-\alpha(\ell-1)\gamma^2/2)$. The width of the distribution decreases as the square root of the number of layers and becomes arbitrarily narrow as the number of layers tends to infinity.

Now consider the effects of nonzero but small ϵ , so that a nonzero fraction of tablets nucleate that are misoriented. The intuitive picture of the process in this regime is that the distribution of angles gets narrower unless nucleation of misoriented tablets occurs. The misorientations prevent the peak from narrowing indefinitely, so after many layers $\phi_\ell(\gamma)$ approaches a stationary distribution that does not change as ℓ increases further. Since a fraction ϵ of tablets is misoriented at each layer, one might expect that the peak in the distribution narrows for $\sim (1/\epsilon)$ layers, so that this naive argument leads to the expectation that the eventual width of the distribution should be proportional to $\epsilon^{1/2}$. However, it is shown below that the subtle interplay between the effects of mutation and selection results in a peak width that can be exponentially small in ϵ as $\epsilon \rightarrow 0$. The high degree of tablet orientation obtained using this mechanism could be a significant advantage in the biological context.

3.1. Steady state behavior of the model

First we find the fixed point behavior for this model, in which the probability distribution function $\phi_\ell(\gamma)$ approaches a limit $\phi^*(\gamma)$ that is independent of ℓ . We expect that this fixed point distribution is reached in the limit $\ell \rightarrow \infty$.

The equation determining the fixed point probability distribution $\phi^*(\gamma)$ is

$$\phi^*(\gamma) = \epsilon f(\gamma) + \frac{1}{N^*}(1 - \epsilon)\phi^*(\gamma)w(\gamma) , \quad (7)$$

with

$$N^* = \int_0^\pi d\gamma \phi^*(\gamma)w(\gamma) . \quad (8)$$

The solution to this equation is

$$\phi^*(\gamma) = \frac{\epsilon f(\gamma)}{1 - \frac{1-\epsilon}{N^*} w(\gamma)}, \quad (9)$$

with

$$N^* = \int_0^\pi d\gamma \epsilon f(\gamma) w(\gamma) \sum_{m=0}^{\infty} \left[\frac{1-\epsilon}{N^*} w(\gamma) \right]^m. \quad (10)$$

We now define

$$v = \frac{1-\epsilon}{N^*}, \quad (11)$$

$$I_m = \int_0^\pi d\gamma (w(\gamma))^{m+1} f(\gamma), \quad (12)$$

and rewrite Eq. (10) as

$$\frac{1-\epsilon}{v} = \epsilon \sum_{m=0}^{\infty} v^m I_m. \quad (13)$$

A useful explicit form for the area distributions can be obtained in the parameter regime in which ϵ , the fraction of misaligned tablets, is small. When $\epsilon \ll 1$, the right hand side of Eq. (13) can be of order unity only if $v^m I_m$ decays slowly for large arguments. Because of its definition, $v > 0$, and it will be seen below that normalization of the probability implies that $v \leq 1$. Therefore, when $m \gg 1$, because $w(\gamma)$ has a single maximum at $\gamma = 0$, the integrand in I_m from Eq. (12) is very sharply peaked near $\gamma = 0$. Therefore, the integration interval can be extended to $[0, \infty]$, one can assume that $w(\gamma)$ is a Gaussian, $w(\gamma) = \exp(-\alpha\gamma^2/2)$, and only the behavior of $f(\gamma)$ for small γ is relevant. If the orientations of the misoriented tablets are chosen uniformly at random in three-dimensional space, then, as discussed in Appendix A, $f(\gamma)$ is proportional to γ as $\gamma \rightarrow 0$, and for small argument $f(\gamma) = \beta\gamma$ (with β a constant of order unity), so that $I_m = \beta \int_0^\infty d\gamma \gamma \exp(-\alpha(m+1)\gamma^2/2) = \beta/(\alpha(m+1))$. Therefore, when $\epsilon \ll 1$,

$$\frac{1-\epsilon}{v} = \epsilon \frac{\beta}{\alpha} \sum_{m=0}^{\infty} \frac{v^m}{m+1}. \quad (14)$$

(Eq. 14 makes it particularly clear that a solution is possible only if $v \leq 1$.) Using the identity [32]

$$\sum_{k=1}^{\infty} \frac{x^k}{k} = -\ln(1-x), \quad (15)$$

one finds

$$\frac{1-\epsilon}{\epsilon} \frac{\alpha}{\beta} = -\ln(1-v), \quad (16)$$

so that

$$N^* = \frac{1-\epsilon}{v} \approx (1-\epsilon) \left(1 + \epsilon \left[-\frac{\alpha(1-\epsilon)}{\beta\epsilon} \right] \right). \quad (17)$$

Therefore, $\phi^*(\gamma)$ can be written

$$\phi^*(\gamma) = \frac{\epsilon f(\gamma)}{1 - \left(1 - \exp\left[-\frac{\alpha(1-\epsilon)}{\beta\epsilon}\right] \exp[-\alpha\gamma^2/2]\right)}. \quad (18)$$

The width of the probability distribution $\phi^*(\gamma)$ in γ , estimated by finding the value of γ at which $\phi^*(\gamma) = \phi^*(0)/2$, is

$$\gamma_{1/2} = \sqrt{\frac{2}{\alpha}} e^{-(1-\epsilon)\alpha/(2\beta\epsilon)}, \quad (19)$$

which is extremely small when ϵ is small.

3.2. Dynamics of the analytic model

The dynamics of the model defined in Eq. (5) can of course be obtained numerically. Analytic insight can also be obtained, following Ref. [18], by writing Eq. (7) for the fixed point function as

$$\phi^*(\gamma) = \epsilon f(\gamma) \sum_{m=0}^{\infty} \left(\frac{1-\epsilon}{N^*} w(\gamma)\right)^m, \quad (20)$$

and comparing this expression to the solution to Eq. (5), which can be written

$$\phi_\ell(\gamma) = \epsilon f(\gamma) \left[\sum_{m=1}^{\ell-1} \prod_{n=1}^{m-1} \left(\frac{1-\epsilon}{N_n} w(\gamma)\right) + \prod_{n=1}^{\ell} \left(\frac{1-\epsilon}{N_n} w(\gamma)\right) \phi_1(\gamma) \right]. \quad (21)$$

If one assumes that the term proportional to $\phi_1(\gamma)$ is negligible and that the normalizations N_n can be approximated as being the same, $N_n = \mathcal{N}$, independent of n , then one obtains an expression for $\phi_\ell(\gamma)$:

$$\phi_\ell(\gamma) \approx \epsilon f(\gamma) \sum_{m=1}^{\ell-1} \left(\frac{1-\epsilon}{\mathcal{N}} w(\gamma)\right)^m. \quad (22)$$

This expression is the sum of contributions that can be interpreted as describing the contribution of the population that has undergone a given number of selection events since the last mutation, and Ref. [18] shows that it agrees well with numerical solutions of Eq. (5).

4. Relating the parameters in the effective theory of Sec. 3 to the parameters in the growth model of Subsec. 2.1.

Sec. 3 presents an analysis of a theory in which one writes an equation for $\phi_\ell(\gamma)$, the fraction of the area in layer ℓ in which the tablet orientation angle is γ . The model analyzed there contains three parameters. The first, α , defined in Eq. 4, governs the degree to which tablets with small values of γ grow faster than tablets with larger values of γ . The second, ϵ , is the fraction of nucleation sites that have tablets with a random orientation instead of the same orientation as the tablet below. The third parameter, β , specifies the width of the distribution governing the distribution of angles of the

misoriented tablets. In contrast, the original growth model described in Subsec. 2.1 has two parameters, ϵ , the fraction of misoriented tablets, and δ , which governs the range of in-plane growth speeds of the misoriented tablets. This section describes the relationships between the two sets of parameters.

The value of ϵ is the same in the analytic theory for orientations as in the growth model (hence the use of the same symbol). The parameters β and δ are related in a straightforward fashion, as discussed below in subsection 4.2. Most of this section will focus on the third parameter in the effective theory, α , which we show depends on the geometry of the nucleation sites in the growth model in subsection 4.3. We will present a simple mean-field theory for estimating the value of α for uncorrelated and random nucleation site locations which yields the correct order of magnitude for the value in subsection 4.3.1. We compare the mean field predictions with the results of simulations of the growth model in subsection 4.3.2.

4.1. Analytic theory for model formulated in terms of tablet growth rates

In the growth model that is simulated numerically, the tablet orientation angles are not considered explicitly because the calculation is formulated using tablet growth rates, and the simulation is performed by choosing an initial configuration of nucleation sites with a distribution of growth rates, and then allowing the tablets to grow from these nucleation sites until they reach confluence. We choose to define a new variable x that ranges between 0 and 1, and define $\mathcal{P}_\ell(x)$, the probability distribution describing the relative frequencies of tablets in layer ℓ with different values of x [16]. It is natural to interpret x as v/v_{max} , where v is the in-plane tablet growth speed and v_{max} is the tablet growth velocity at the orientation where this velocity is maximum.

As discussed above and in Appendix A, when the model is formulated in terms of orientation angles, the “fitness” function specifying the changes in the fractions of the area covered by tablets with different angles of misorientation between successive layers is expected to have a quadratic maximum at $\gamma = 0$. Because the tablet growth velocity itself depends quadratically on γ near $\gamma = 0$ (again, because misorientations by γ and $-\gamma$ are equivalent and so yield the same growth velocity), the “fitness” function that specifies the change in relative area of the different values of x , $\tilde{w}(x)$, depends linearly on x near $x = 1$. Recalling that the probability distributions in the model are normalized, so that the overall scale of $\tilde{w}(x)$ is arbitrary, and that the behavior is dominated by the behavior near $x = 1$, two ways of parameterizing this dependence are to (1) fix the value of $\tilde{w}(1) = 1$ and specify the slope \tilde{w}' , or (2) to write $\tilde{w}(x) = x^\xi$ and specify ξ . These two forms are equivalent near $x = 1$, with $\tilde{w}'(x) = \xi$; we will choose to use the power-law form $\tilde{w}(x) = x^\xi$.

To obtain additional insight into the relationship between the two formulations of the model, we reformulate the analytic theory in terms of the variable x (this formulation is very similar to that in Ref. [16]). Assuming that tablets with normalized growth rate x grow to have an area that is proportional to x^ξ for some ξ , and assuming that there

the probability of nucleation of a misoriented tablet is ϵ , the probability distribution for the tablet growth velocities in layer ℓ , \mathcal{P}_ℓ , obeys

$$\mathcal{P}_{\ell+1}(x) = \epsilon g(x) + (1 - \epsilon)(1/\mathcal{N}_\ell)x^\xi \mathcal{P}_\ell(x) , \quad (23)$$

where $g(x)$ is the probability distribution for the misoriented tablets and $\mathcal{N}_\ell = \int_0^1 dx x^\xi \mathcal{P}_\ell(x)$. Using methods precisely analogous to those in the previous section, we write the equation for fixed point reached at large ℓ , $\mathcal{P}^*(x)$:

$$\begin{aligned} \mathcal{P}^*(x) &= \frac{\epsilon g(x)}{1 - \frac{(1-\epsilon)}{\mathcal{N}^*} x^\xi} \\ &= \epsilon g(x) \sum_{m=0}^{\infty} \left(\frac{(1-\epsilon)}{\mathcal{N}^*} x^\xi \right)^m , \end{aligned} \quad (24)$$

where \mathcal{N}^* obeys

$$\begin{aligned} \mathcal{N}^* &= \int_0^1 dx \mathcal{P}^*(x) \\ &= \int_0^1 dx \epsilon g(x) \sum_{m=0}^{\infty} \left(\frac{(1-\epsilon)}{\mathcal{N}^*} x^\xi \right)^m . \end{aligned} \quad (25)$$

When ϵ is small, then the integrals are dominated by the region where x is close to unity, and the x -dependence of $g(x)$ can be neglected, yielding

$$\mathcal{N}^* = \epsilon g(1) \sum_{m=0}^{\infty} \left(\frac{1-\epsilon}{\mathcal{N}^*} \right)^m \frac{1}{1 + \xi m} . \quad (26)$$

When ϵ is small, so that v is close to 1, this sum is dominated by the region in which $\xi m \gg 1$, and, using $\sum_{k=1}^{\infty} x^k/k = -\ln(1-x)$, one obtains

$$\mathcal{N}^* = -\frac{\epsilon g(1)}{\xi} \ln \left(1 - \frac{1-\epsilon}{\mathcal{N}^*} \right) . \quad (27)$$

Recalling that \mathcal{N}^* is extremely close to $1 - \epsilon$, one obtains

$$1 - \epsilon = -\frac{\epsilon g(1)}{\xi} \ln \left(1 - \frac{1-\epsilon}{\mathcal{N}^*} \right) , \quad (28)$$

so that

$$\mathcal{N}^* = (1 - \epsilon) \left(1 + \exp - \left(\frac{(1-\epsilon)\xi}{\epsilon g(1)} \right) \right) \quad (29)$$

and

$$\mathcal{P}^*(x) = \frac{\epsilon g(x)}{1 - \left(1 - \exp \left[-\frac{(1-\epsilon)\xi}{\epsilon g(1)} \right] \right) x^\xi} . \quad (30)$$

This form is consistent with Eq. (18). Comparing the forms, one can see that the parameter α in the effective model enters into Eq. (18) in a way similar to that in which ξ enters into Eq. (30), and that β enters into Eq. (18) in a way similar to that in which $g(1)$ enters into Eq. (30).

4.2. Relationship between parameters β and δ .

The parameter β in the analytic model and the parameter δ in the growth model each describe the probability distribution governing the misoriented tablets. As seen above, because of the action of the “selection” in the model, the key property of these distributions is their behavior near $\gamma = 0$ and $x = 1$. Therefore, we work out the relationship between the two formulations of the model in this region.

For the growth model, the distribution of the in-plane growth speed v is chosen to be uniform in the range $[1 - \delta/2, 1 + \delta/2]$, so the probability density in terms of the variable v is $1/\delta$. To convert to x , the normalized growth speed, we note that the maximum growth velocity is $1 + \delta/2$, so that the probability density for x is $(1/\delta)(dv/dx) = (1 + \delta/2)/\delta$. For the analytic formulation of the theory, choosing this distribution to be $f(\gamma) = \beta\gamma e^{-\beta\gamma^2/2}$ (the coefficient is determined by normalizing $\int_0^{\pi/2} f(\gamma)d\gamma = 1$, and assuming that β is large enough that setting the upper limit of the integration at ∞ introduces negligible error), the probability density near $\gamma = 0$ is $f(\gamma) \rightarrow \beta\gamma$. Near $\gamma = 0$, the variables γ and x are related by $x = 1 - A\gamma^2$, for some constant A , so near $\gamma = 0$ we can write

$$\begin{aligned} d\gamma f(\gamma) &\approx dx(1 + \delta/2)\delta \\ dx(d\gamma/dx)(\beta\gamma) &\approx dx(1 + \delta/2)/\delta \\ (\beta\gamma)/(2A\gamma) &\approx (1 + \delta/2)/\delta, \end{aligned} \tag{31}$$

leading to the identification $\beta/(2A) = (1 + \delta/2)/\delta$. This relationship between the probability distributions of the orientation angles and the growth speeds involves not just β and δ but also a new constant A , that specifies the relationship between the change in orientation angle and the change in growth speed. However, this constant A also enters into the “fitness” or “selection” term that is discussed in the next subsection in precisely analogous fashion, so that the relationship between ratios α/β and $\xi/g(1)$ in Eqs. (18) and Eq. (30) does not depend on A .

4.3. Dependence of α on geometry

This subsection discusses how the parameter α in Eq. 4 is related to the growth model as described in Subsec 2.1. It can be seen that α does not depend on ϵ and δ by noting that in the limit of $\epsilon \rightarrow 0$, when no misoriented tablets are nucleated, both ϵ and δ drop out of the model altogether, while the selection term in which α appears still operates. We will see that the value of α is essentially determined by geometrical considerations only.

The value of α in the analytic model depends on the geometric arrangement of nucleation sites in the growth model. This is because the areas of the tablets after growth is completed depend on the differences between growth rates of neighboring tablets as opposed to depending on individual growth rates themselves; two neighboring tablets growing at the same speed will not lose area to each other, no matter what that rate happens to be. Changes in the fractions of area covered by tablets with different growth rates arise only when fast-growing tablets are next to slow-growing tablets. In

fact, if one considers a one-dimensional case of N tablets in which the growth rate of tablet j is $g_0 + cj$, where $g > 0$ and c are constants, it is easy to see that there is a set of locations for the nucleation sites such that the size of every tablet stays the same except for the tablets at $j = 1$ and $j = N$.

Here we consider the specific case of a collection of uncorrelated, randomly chosen nucleation sites. For this situation, neighboring tablets are likely to have different growth speeds, so that the differential growth rates will lead to fast-growing tablets increasing their share of the area. We first present a simple mean field estimate for the resulting value of α , and then present numerical computations that can be used to extract its value.

4.3.1. Mean field theory for α for random nucleation sites In this subsection we construct a simple mean-field theory for estimating α . In the next subsection we will compare the mean-field theory results with the results obtained using numerical simulations.

In subsection 4.1 we showed that without loss of generality, one can choose the form for the selection term in the growth model for the relative area covered by tablets with normalized growth speed x to be x^ξ . Here we present a simple mean-field theory for calculating ξ using arguments very similar to those typically used in statistical physics [33]: We assume that when a tablet grows, it does so in the presence of neighbors with *mean* properties. and take account explicitly of the fact that faster-growing tablets will tend to reach confluence with their neighbors sooner than slower-growing ones. One assumes that when a given tablet grows, it does so in the presence of neighbors that have *average* properties.

Given that a tablet has normalized growth speed $x = v/v_{max}$ and that the mean normalized growth speed is $\bar{x} = \bar{v}/v_{max}$, then we wish to calculate the area covered by the tablet after it has grown to confluence with its neighbors. For simplicity, we will consider nucleation sites that are placed on a regular lattice (or alternatively, consider the scaling of the behavior without worrying about numerical coefficients). For two nucleation sites separated by d with normalized growth rates x_1 and \bar{x} , the time for the tablets to grow to confluence is proportional to $d/(x_1 + \bar{x})$, so the area of the tablet in question should scale as $x_1^2/(x_1 + \bar{x})^2$. Therefore, the ratio of the area taken up by the tablet we are considering to that of the “mean-field” tablet (which we assume has area that scales as $\bar{x}^2/(x_1 + \bar{x})^2$) is x_1^2/\bar{x}^2 . Approximating \bar{x} as constant (which is reasonable because the probability distribution for x is asymmetric, monotonically decreasing from $x = 1$, with a mean very near 1) yields the result that the area growth for a normalized velocity x_1 is proportional to x_1^2 , so that $\xi = 2$.

A modification of this mean field theory, that yields a value for ξ that agrees better with the results of the numerical simulations below, is obtained by noting that while the area of the tablet under consideration is proportional to $x_1^2/(x_1 + \bar{x})^2$, the area of the mean-field neighbors varies little when x_1 changes because their interactions with their other neighbors are not affected. Assuming that the change in areas of the “mean-field”

tablets can be neglected altogether yields the value $\xi = 1$. This result can be seen in several ways: first, the mean-field argument given just above assumes that increasing x_1 leads to a decrease in the “mean-field” tablet area that scales the same way as the increase in the area of the “non-mean-field” tablet, so ignoring the former contribution leads to a result that is the square root of the one obtained previously. Alternatively, one can argue as follows: since the area growth of the “non-mean-field” tablet growing with normalized velocity x_1 is proportional to $x_1^2/(x_1 + \bar{x})^2$, we can write $x_1 = 1 - \rho_1$, $\bar{x} = 1 - \bar{\rho}$, assume that ρ_1 and $\bar{\rho}$ are each $\ll 1$, and fix the proportionality constant by requiring the relative area to be unity when $x_1 = 1$. When $\bar{\rho}$ is close to unity, this procedure also yields the result $\xi = 1$.

4.3.2. Numerical evaluation of parameters in effective theory for synchronous nucleation and random nucleation geometry For the simulations presented in this section, the initial distribution of tablet growth velocities tablets are chosen to be uniform in the range $[1 - \delta/2, 1 + \delta/2]$, or, equivalently, $g(x) = 1/\delta$ for x in the range $[(1 - \delta/2)/(1 + \delta/2), 1]$. Because the focus is on determining the value of α in the selection term of the effective model, the parameter ϵ is set to zero in the simulations in this section.

The comparison between mean field theory and simulation is done by comparing $x_{1/2}(\ell)$, the median growth speed found in the simulation at layer ℓ , to the median of the distribution found using the analytic mean-field theory, which satisfies

$$\int_0^{x_{1/2}(\ell)} \mathcal{P}_\ell(x) dx = 1/2 . \quad (32)$$

When $\epsilon = 0$, the dynamical equation for $\mathcal{P}_\ell(x)$ is

$$\mathcal{P}_{\ell+1}(x) \propto x^\xi \mathcal{P}_\ell(x) , \quad (33)$$

which has the solution

$$\mathcal{P}_\ell(x) = x^{\xi\ell} \mathcal{P}_0(x) . \quad (34)$$

When ℓ is large, the x -dependence of $\mathcal{P}_0(x)$ can be neglected, and one obtains $\mathcal{P}_\ell(x) \propto x^{\xi\ell}$, yielding a normalized distribution $\mathcal{P}_\ell(x) = (\xi\ell + 1)x^{\xi\ell}$. The median value of this distribution, $x_{1/2}(\ell)$, is

$$\begin{aligned} x_{1/2}(\ell) &= \left(\frac{1}{2}\right)^{\frac{1}{\xi\ell+1}} \\ &\approx 1 - \frac{\ln 2}{\xi\ell + 1} . \end{aligned} \quad (35)$$

Therefore, when ℓ is large, the slope of the plot of the median value $x_{1/2}(\ell)$ versus $1/\ell$ approaches $\ln(2)/\xi$, providing a method for extracting the value of ξ from numerical simulations.

The procedure used for the numerical simulations is very similar to that used for those presented in Ref. [8], but specialized to the limit in which successive layers nucleate much more slowly than individual layers grow to completion. Each layer in

the simulation is a square of dimension 400×400 (the length unit is arbitrary, and is adjusted to agree with measured tablet widths when numerical results are compared with experimental data in Ref. [8,15]) with nucleation sites whose sites are independently and randomly chosen from a probability distribution with uniform spatial density. Open boundary conditions were employed. The growth rates in the initial layer are chosen uniformly at random in the interval $[1 - \delta/2, 1 + \delta/2]$ (resulting in normalized growth rates in the interval $[(1 - \delta/2)/(1 + \delta/2), 1]$). In these simulations, the parameter ϵ is set to zero (no misoriented tablets are nucleated).

4.3.3. Numerical results As discussed in Sec. 4.3.2, the value of ξ that determines the strength of the “selection” can be extracted by computing the median value of the in-plane tablet growth velocity, $x_{med}(\ell)$ as a function of layer number ℓ , when $\epsilon = 0$. Eq. (35) predicts that the quantity $1/(1 - x_{med}(\ell))$ depends linearly on ℓ , and the slope of this dependence is $\xi/\ln 2$. For the uniform distribution of growth rates used in the numerical simulations, the initial value of this quantity, $1/(1 - x_{med}(1))$, is $1 + 2/\delta$.

Figure 2 is a plot of the quantity $1/(1 - x_{med}(\ell))$ as a function of layer number ℓ for different values of δ . The graph also shows the dependence expected for $\delta = 0.3$ using the two different mean-field results obtained above, $\xi = 2$ and $\xi = 1$. There is substantial scatter in the numerical data, but it appears that the behavior is consistent with the value $\xi = 1$ but not with the value $\xi = 2$.

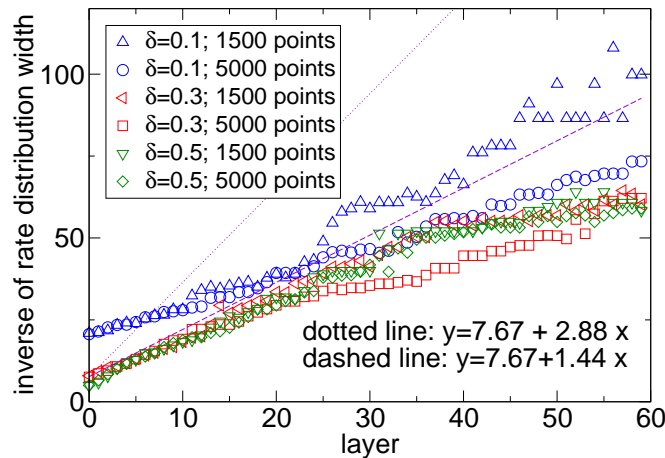


Figure 2. Plots of $1/(1 - x_{med}(\ell))$ versus layer number ℓ , obtained by numerical simulation of the model, where $x_{med}(\ell)$ is the median value of normalized growth speed x in layer ℓ . The number of nucleation points per layer and the value of δ for each run are shown in the legend. For the uniform distribution of growth rates used in the numerical simulations, the initial value of the ordinate, $1/(1 - x_{med}(1))$, is $1 + 2/\delta$. The mean field theories described in the text yield a linear dependence for this quantity, one with slope $2/\ln 2 \approx 2.88$, corresponding to the value $\xi = 2$ (a dotted line with this slope is shown on the plot), and the other with slope $1/\ln 2 \approx 1.44$ (dashed line on the plot). The numerical results exhibit considerable scatter, but appear to be consistent with the value of $\xi = 1$ and not the value of $\xi = 2$.

5. Discussion

In this paper we have detailed investigations of a model for the development of orientational order of the aragonite tablets in nacre. The model is investigated both by direct numerical simulation and by analysis of the evolution of the probability distribution governing tablet orientations that is analogous to mutation-selection theories studied in population biology. The relationships between the parameters in the version of the model used for the numerical simulations and those in the version used for the analytic work are investigated.

The model simulated in this paper can be extended in many ways to model nacre growth more realistically. In Ref. [8] the model is modified to take the columnar growth of abalone nacre into account, by restricting each nucleation site to be within a given distance from a nucleation site in the layer below, as opposed to the model used in this paper, in which the nucleation sites in each layer are chosen independently and randomly in the simulational domain. Compared to the version in Ref. [8], the model examined here has the advantage that it has one less parameter. Because the analytic theory is constructed using very general symmetry considerations, it is clear that the qualitative behavior of a model implementing columnar growth is the same as for the model studied here. Similarly, the growth model can be generalized in other ways (for instance, by implementing more realistic microscopic growth rates with explicit modeling of three-dimensional growth or by considering asynchronous nucleation) will still yield the same analytic model, though with possibly different values for the model parameters.

The relationships between the parameters in the analytic theory and in the growth model presented in Subsec. 2.1 were investigated using a mean field theory and by numerical simulation. Two mean field theories were constructed to estimate the parameter describing the strength of the tendency for faster-growing tablets to take up more area than slower-growing ones. Numerical simulations of the growth model yield a result for this parameter that agree reasonably well with one of the mean field theories. Development of a more sophisticated analytic theory for calculating the value for this parameter is an interesting open problem.

6. Conclusions

This paper investigates theoretically a model for the development of orientational order of the aragonite tablets in nacre, or mother-of-pearl. Motivated by experiments demonstrating the this ordering develops over many tens of layers, the model assumes that the tablet growth rates depend on the orientation of their c-axes, with tablets with c-axis orientation normal to the layer plane growing the fastest. This model is closely related to mutation-selection models used in population biology.

A combination of analytic and numerical results were applied to analyze the model. It is shown that the model yields a degree of ordering that is extremely good when the parameter ϵ , that governs the fraction of tablets with nucleate with misoriented c-axes,

is small.

7. Acknowledgments

We gratefully acknowledge for this research provided by NSF-DMR and by DOE. S.N.C. acknowledges the hospitality of the Aspen Center for Physics, where some of the work was performed.

Appendix A. Form of functions used in analytic model

This appendix discusses the forms of the functions $w(\gamma)$ and $f(\gamma)$ that are used in Sec. 3 to specify the model for the evolution of the probability distribution of tablet orientations. The function $w(\gamma)$ specifies the tendency of the area covered by faster-growing tablets to increase, while $f(\gamma)$ specifies the probability distribution function for the angles of the misoriented tablets. We assume that the growth rate is isotropic in the a-b plane, so that the tablet growth velocity depends only on γ , the angle between the c-axis orientation of the tablet and the layer normal.

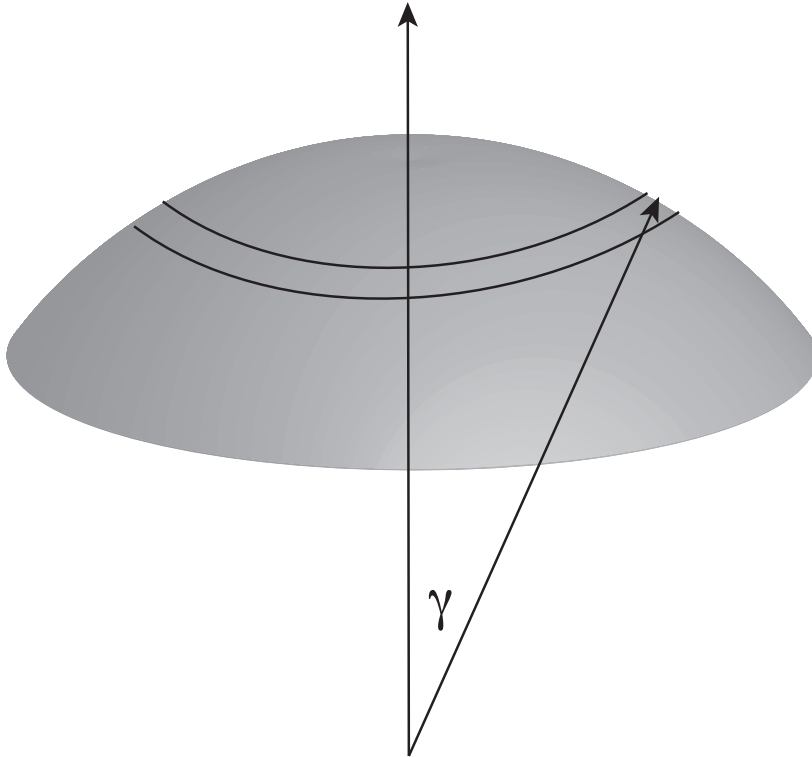


Figure A1. Schematic of geometry, illustrating that assuming that the c-axes of misoriented tablets are equally likely to have any orientation, then the function $f(\gamma)$ introduced in Sec. 3 is proportional to γ as $\gamma \rightarrow 0$.

For the function $w(\gamma)$, our assumption that the growth speed has no azimuthal dependence implies that the growth speed of a tablet with crystal axis misoriented from

the layer normal by an angle γ is a function of $\cos(\gamma)$ and has a quadratic maximum at $\gamma = 0$. When the parameter ϵ governing the fraction of misoriented tablets is small, the dynamics is controlled by the behavior for small γ . As discussed in the main text, it is often convenient to choose $w(\gamma)$ to be a Gaussian, which makes calculation of its dynamical effects particularly simple.

Now we discuss the function $f(\gamma)$ that describes the distribution of misoriented tablets. If one makes the simplest assumption that the orientations of these misoriented tablets take on each angle with equal probability, then the probability distribution for γ , the angle between the tablet c-axis orientations and a fixed external axis (here, the direction of the layer normal) is proportional to $\sin(\gamma)$, since the area of a spherical surface between angles γ and $\gamma + d\gamma$ is proportional to $\sin(\gamma)d\gamma$, or $d\cos(\gamma)$. The relevant geometry is shown in Fig. 3.

As discussed in the main text, the model can be formulated entirely in terms of tablet growth rates, and we use such a form in our numerical simulations. We define the variable x to be the normalized tablet growth rate, with $x = 1$ the maximum value. Because (1) we assume that the tablet growth rate exhibits a quadratic maximum at $\gamma = 0$, and (2) the area between the angles γ and $\gamma + d\gamma$ is proportional to γ as $\gamma \rightarrow 0$, in terms of x , the growth rate is maximum at $x = 1$ and depends linearly on x near $x = 1$. Similarly, the function describing the relative change in area taken up by tablets with c-axis orientation γ , $w(\gamma)$, has a quadratic maximum as a function of γ , so the analogous function expressed in terms of the growth rate will depend linearly on x near $x = 1$.

References

- [1] S. Mann. *Biom mineralization: Principles and Concepts in Bioinorganic Materials Chemistry*. Oxford University Press, Oxford, 2001.
- [2] F. Nudelman, B. A. Gotliv, L. Addadi, and S. Weiner. Mollusk shell formation: Mapping the distribution of organic matrix components underlying a single aragonitic tablet in nacre. *Journal of Structural Biology*, 153(2):176–187, 2006.
- [3] I. M. Weiss and V. Schonitzer. The distribution of chitin in larval shells of the bivalve mollusk *mytilus galloprovincialis*. *Journal of Structural Biology*, 153(3):264–277, 2006.
- [4] N. Nassif, N. Gehrke, N. Pinna, N. Shirshova, K. Tauer, M. Antonietti, and H. Colfen. Synthesis of stable aragonite superstructures by a biomimetic crystallization pathway. *Angewandte Chemie-International Edition*, 44(37):6004–6009, 2005.
- [5] M. Rousseau, E. Lopez, A. Coute, G. Mascarel, D. C. Smith, R. Naslain, and X. Bourrat. Sheet nacre growth mechanism: a Voronoi model. *Journal of Structural Biology*, 149(2):149–157, 2005.
- [6] J. D. Currey. Mechanical properties of mother of pearl in tension. *Proceedings of the Royal Society of London Series B-Biological Sciences*, 196(1125):443–463, 1977.
- [7] Rebecca A. Metzler, Mike Abrecht, Ronke M. Olabisi, Daniel Ariosa, Christopher J. Johnson, Bradley H. Frazer, Susan N. Coppersmith, and P. U. P. A. Gilbert. Architecture of columnar nacre, and implications for its formation mechanism. *Physical Review Letters*, 98(26):268102, 2007.
- [8] P.U.P.A Gilbert, Rebecca A. Metzler, Dong Zhou, Andreas Scholl, Andrew Doran, Anthony Young, Martin Kunz, Nobumichi Tamura, and S.N. Coppersmith. Gradual ordering in red abalone nacre. *J. Am. Chem. Soc.*, 130:17519–17527, 2008.

- [9] Y. Levi-Kalisman, G. Falini, L. Addadi, and S. Weiner. Structure of the nacreous organic matrix of a bivalve mollusk shell examined in the hydrated state using cryo-TEM. *Journal of Structural Biology*, 135(1):8–17, 2001.
- [10] T. E. Schaffer, C. Ionescu-Zanetti, R. Proksch, M. Fritz, D. A. Walters, N. Almqvist, C. M. Zaremba, A. M. Belcher, B. L. Smith, G. D. Stucky, D. E. Morse, and P. K. Hansma. Does abalone nacre form by heteroepitaxial nucleation or by growth through mineral bridges? *Chemistry of Materials*, 9(8):1731–1740, 1997.
- [11] F. Song and Y. L. Bai. Effects of nanostructures on the fracture strength of the interfaces in nacre. *Journal of Materials Research*, 18(8):1741–1744, 2003.
- [12] E. DiMasi and M. Sarikaya. Synchrotron x-ray microbeam diffraction from abalone shell. *Journal of Materials Research*, 19(5):1471–1476, 2004.
- [13] L. Addadi and S. Weiner. Interactions between acidic proteins and crystals - stereochemical requirements in biomineralization. *Proceedings of the National Academy of Sciences of the United States of America*, 82(12):4110–4114, 1985.
- [14] R.A. Metzler, M. Abrecht, J.-W. Chiou, J. Guo, D. Ariosa, S.N. Coppersmith, and P.U.P.A. Gilbert. Polarization-dependent imaging contrast in abalone shells. *Physical Review B*, 77:064110, 2008.
- [15] Rebecca A. Metzler, Dong Zhou, Mike Abrecht, Susan N. Coppersmith, and P.U.P.A. Gilbert. Ordering in red abalone nacre, preprint arxiv:0710.4573, 2007.
- [16] J. F. C. Kingman. A simple model for the balance between selection and mutation. *Journal of Applied Probability*, 15:1–12, 1978.
- [17] M. Turelli. Heritable genetic variation via mutation selection balance - lerch zeta meets the abdominal bristle. *Theoretical Population Biology*, 25(2):138–193, 1984.
- [18] S. N. Coppersmith, Robert D. Blank, and Leo P. Kadanoff. Analysis of a population genetics model with mutation, selection, and pleiotropy. *Journal of Statistical Physics*, 97:429–457, 1999. preprint cond-mat/9809143.
- [19] M. Kimura. A stochastic model concerning maintenance of genetic variability in quantitative characters. *Proceedings of the National Academy of Sciences of the United States of America*, 54(3):731–736, 1965.
- [20] M. C. Cross and P. C. Hohenberg. Pattern formation outside of equilibrium. *Reviews of Modern Physics*, 65(3):851–1112, 1993.
- [21] R. Burger and I. M. Bomze. Stationary distributions under mutation-selection balance: Structure and properties. *Advances in Applied Probability*, 28(1):227–251, 1996.
- [22] D. Waxman and J. R. Peck. Pleiotropy and the preservation of perfection. *Science*, 279(5354):1210–1213, 1998.
- [23] M. Fritz, A. M. Belcher, M. Radmacher, D. A. Walters, P. K. Hansma, G. D. Stucky, D. E. Morse, and S. Mann. Flat pearls from biofabrication of organized composites on inorganic substrates. *Nature*, 371(6492):49–51, 1994.
- [24] H. A. Lowenstam and S. Weiner. *On Biomineralization*. Oxford University Press, Oxford, 1989.
- [25] S. Weiner and W. Traub. *Organic-matrix-mineral relationships in mollusk shell nacreous layers*, pages 467–482. Balaban ISS, Rehovot and Philadelphia, 1981.
- [26] J. H. E. Cartwright and A. G. Checa. The dynamics of nacre self-assembly. *Journal of the Royal Society Interface*, 4(14):491–504, 2007.
- [27] Atsuyuki Okabe, Barry Boots, and Kokichi Sugihara. Nearest neighbourhood operations with generalized Voronoi diagrams: a review. *International Journal of Geographical Information Systems*, 8(1):43–71, 1994.
- [28] K. Kobayashi and K. Sugihara. Crystal Voronoi diagram and its applications. *Future Generation Computer Systems*, 18(5):681–692, 2002.
- [29] L. Mu and X. Wang. Population landscape: a geometric approach to studying spatial patterns of the us urban hierarchy. *International Journal of Geographical Information Science*, 20(6):649–667, 2006.

- [30] V. L. Ginzburg and L. D. Landau. On the theory of superconductivity. *Zh. Eksp. Teor. Fiz.*, 20:1064–1082, 1950.
- [31] N. Goldenfeld. *Lectures on Phase Transitions and the Renormalization Group*. Perseus Publishing, Reading, MA, 1992.
- [32] L. Lewin. *Polylogarithms and Associated Functions*. North-Holland, New York, 1981.
- [33] David Chandler. *Introduction to Modern Statistical Mechanics*. Oxford University Press, New York, 1987.